

Agent Journey Beyond RGB: Unveiling Hybrid Semantic-Spatial Environmental Representations for Vision-and-Language Navigation

Xuesong Zhang* Yunbo Xu* Jia Li[†] Zhenzhen Hu Richnag Hong
Hefei University of Technology, Hefei, China

{xs Zhang_hfut, xuyunbo.cn}@mail.hfut.edu.cn, jiali@hfut.edu.cn
{huzhen.ice, hongrc.hfut}@gmail.com.

Abstract

Navigating unseen environments based on natural language instructions remains difficult for egocentric agents in Vision-and-Language Navigation (VLN). Existing approaches primarily rely on RGB images for environmental representation, underutilizing latent textual semantic and spatial cues and leaving the modality gap between instructions and scarce environmental representations unresolved. Intuitively, humans inherently ground semantic knowledge within spatial layouts during indoor navigation. Inspired by this, we propose a versatile Semantic Understanding and Spatial Awareness (SUSA) architecture to encourage agents to ground environment from diverse perspectives. SUSA includes a Textual Semantic Understanding (TSU) module, which narrows the modality gap between instructions and environments by generating and associating the descriptions of environmental landmarks in agent’s immediate surroundings. Additionally, a Depth-enhanced Spatial Perception (DSP) module incrementally constructs a depth exploration map, enabling a more nuanced comprehension of environmental layouts. Experiments demonstrate that SUSA’s hybrid semantic-spatial representations effectively enhance navigation performance, setting new state-of-the-art performance across three VLN benchmarks (REVERIE, R2R, and SOON). The source code will be publicly available.

1. Introduction

With the advancement of multimodal technology [29, 44, 47, 59], several embodied VLN tasks [2, 8, 37, 41] have garnered significant attention due to their promising applications in robotics and intelligent assistance. Among them, conventional VLN tasks [2, 27] focused on step-by-step navigation within unseen environments based on detailed instructions, while goal-oriented VLN tasks [41, 45, 64] demand agents to identify predefined objects based on high-

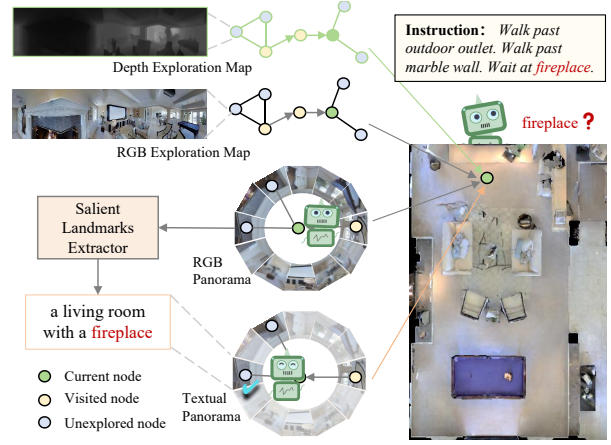


Figure 1. An overview of the proposed SUSA. Unlike previous approaches that solely rely on RGB input, we introduce view-level textual panoramas and trajectory-level depth exploration maps, supporting the agent’s explicit understanding of the environment.

level instructions. Consequently, VLN agents are required to profoundly cognize the spatial information of environment and ground them with textual instructions to brilliantly accomplish arduous navigation tasks.

Considerable literature has exhibited the efficacy of Transformer-based models [5, 20, 38, 40, 52] for interacting with instructions, RGB-based environmental observations, and historical trajectories. However, we suggest that RGB-only visual environment representations leave VLN fraught with two challenges: the modality gap between instructions and the environment, and the scarcity of training environmental representations. Firstly, VLN agents struggle to precisely match the landmarks in language instructions with the entities in visual environments, due to the intrinsic modality heterogeneity. To address this, recent works [12, 32] utilized contrastive learning to promote alignment, while others leveraged candidate object concepts [33, 50], large language models (LLMs) [34] or retrieved knowledge [31] to explicitly reason the textual semantics (*i.e.*, linguis-

*The first and second authors contributed equally to this work.

[†]Corresponding author: jiali@hfut.edu.cn.

tic descriptions about landmarks) to enhance environmental representations. However, these methods do not directly align textual semantics with landmarks (e.g., “fireplace” in Fig. 1) in instruction, yielding trivial gain.

The second challenge pertains to the monotonous and limited environmental representations, which often leads agents to overfit to familiar spatial layouts [51]. To alleviate this limitation, recent endeavors [7, 55] augment the quantity of environmental scenes, while others diversify environmental representations by constructing graphs [16, 23], grids [1, 56], or volumetric environments [36]. However, these RGB-based methods easily suffer from attention imbalance or environmental bias [61, 65]. FDA [18] utilizes frequency information to enrich environmental representations. However, depth images vividly convey spatial information (e.g., doors and corridors), which is often overlooked in discrete navigation tasks [49]. Few works [1, 56] incorporate depth, they merely project depth values onto the corresponding spatial locations of RGB images, rather than independently grounding depth [53]. Overall, the underlying textual semantic and spatial representations remains underutilized, though studies [22] suggest that injecting inductive biases where different modules access distinct modalities, offers a promising solution.

In this work, we propose the Semantic Understanding and Spatial Awareness (SUSA) architecture, which individually grounds semantic and spatial representations of the environment with instructions and synergistically predicts navigation actions from diverse perspectives. As illustrated in Fig. 1, we first construct a view-level textual panorama by extracting salient landmarks as the textual semantics to explicitly match them with language instructions, and select the most instruction-relevant view, thereby bridging the semantic gap between the visual and linguistic modalities. Further, beyond RGB images, we progressively construct an independent trajectory-level depth exploration map to enhance the agent’s spatial perception of the environment, also directly aligning it with instructions. To enable the agent to absorb complementary information from different environmental perspectives, we aggregate these hybrid semantic-spatial environmental representations to synergistically facilitate hierarchical navigation predictions, and employ contrastive learning to align these hybrid representations with language instructions. We empirically substantiate that exclude semantic panoramas and depth exploration maps during pretraining manifest markedly enhanced generalization capabilities. Experimental results demonstrate that our agent achieves significantly improved navigation performance, outperforming state-of-the-art methods across three vision-and-language navigation benchmarks: R2R [2], REVERIE [41], and SOON [64].

The main contributions of our SUSA are as follows:

- SUSA devises a textual-aware semantic understanding

(TSU) module to match the most related landmarks between environments and instructions, explicitly addressing the modality heterogeneity.

- SUSA further presents a depth-enhanced spatial perception (DSP) module to explore and represent environmental layouts beyond surface RGB content.
- Extensive experiments on three VLN benchmarks have demonstrated the superiority of hybrid semantic-spatial environmental representations introduced by SUSA.

2. Related Work

Vision-and-Language Navigation (VLN). Vision-and-Language Navigation (VLN) tasks [2, 41, 64] require an agent to navigate in embodied environments sequentially towards a designated location or object based on natural language instructions. Given that the VLN task can be formulated as a partially observable Markov decision process, early methods [14, 26, 54, 66] primarily relied on reinforcement learning and imitation learning paradigms to improve navigation performance, incorporating various strategies and auxiliary loss [54, 63] designs. More recently, to better generalize to unknown environments and ground instructions, many researchers [5, 20, 38, 40, 52] have focused on transformer-based architectures, which effectively model interactions among instructions, environmental features, and historical navigation trajectories. While these approaches have propelled VLN forward, they mainly rely on fragile RGB-based environment representations. This paper encourages the agent to perceive and ground the environment from text semantics and depth perspectives.

Semantic Alignment in VLN. To align the semantic relationship between the environment and instructions, current practitioners in the VLN community can be divided into two categories: implicit and explicit approaches. Implicit methods [12, 32, 51] commonly employ contrastive learning or attention mechanisms to associate visual contexts with textual instructions. However, given the inherent semantic gap between these modalities, implicit approaches have limited alignment capabilities. Explicit alignment techniques aim to project both semantics into a same modality space. For example, some methods transform the environment into a text-based modality, Console [34] scores landmark co-occurrences to identify key objects, and AACL [33] leverages CLIP [44] to refine textual entities. Similar to our approach, KERM [31] utilizes retrieved knowledge as textual semantics for each view. However, these explicit methods directly “stitch” textual and visual environment representations, which may lead to an overreliance on text modality yet underutilizing visual data [67]. We thus take environmental textual semantic as an independent modality to directly match the most instruction-relevant landmarks.

Environment Representations in VLN. Limited training sources and environmental representations in VLN tasks

hinder the agent to generalize the unknown layouts. Prior endeavors mitigate this limitation through data augmentation [35, 55] or by diversifying visual representations [1, 36, 56, 60]. However, these approaches primarily rely on RGB images, while alternative modalities such as frequency [18], spectral [24], depth [49] and semantic information [4, 21, 53] remain relatively underexplored. Among them, SEAT [53] enhances cross-domain environmental perception by querying the Matterport3D simulator [3] for depth and semantics. However, SEAT fuses these multi-type representations into a unified space without explicitly grounding each modality. Moreover, these semantic representations [21, 53] are not inherently textual, limiting their ability to bridge the modality gap. In contrast, our method constructs the view-level textual panoramas and trajectory-level depth exploration maps, directly grounding them with instructions to perceive rich environmental representations.

3. Methodology

3.1. Preliminary

Task Formulation. We focus on discrete VLN tasks [2, 41, 64] within a Matterport3D simulator [3], modeled as an undirected graph $\mathcal{G} = \{\mathcal{N}, \mathcal{E}\}$, where \mathcal{N} denotes nodes and \mathcal{E} signifies the connectivity paths. At the outset of each episode, the agent equipped with a GPS sensor, RGB and depth cameras, is situated at a randomly navigable node and receives a language instruction $I = \{w_i\}_{i=1}^l$ including l words. We use BERT [10] to extract instruction features and then embed them as $\mathcal{I} = \{w_1, \dots, w_l\}$. At each time step t , the agent can perceive the surrounding RGB panorama $R_t = \{r_{t,i}\}_{i=1}^{n=36}$ and depth panorama $D_t = \{d_{t,i}\}_{i=1}^{n=36}$ along with n corresponding views. During navigation, the agent make the next action a_t by selecting one navigable node from the candidate actions $\mathcal{A}_t = \{a_{t,i}\}_{i=0}^k$. The sequential decision-making process is iterated until the agent decides to stop at the current location or exceeds the maximum navigation steps. For goal-oriented tasks [41, 64], the agent is also tasked with locating a target object.

Overview of the Proposed Method. Our objective is to accord complementary environmental content by equipping the agent with a textual semantic panorama and a depth exploration map. Following prevailing approaches [18, 19, 30], we adopt DUET [6] as our baseline, which merely utilizes RGB panoramas and topological maps as environmental representations for both local and global action predictions. The SUSA framework consists of three main modules: (a) textual-aware semantic selection is detailed in Sec. 3.2, (b) depth-aware visual environment exploration is presented in Sec. 3.3, and (c) hybrid representation aggregation and hierarchical action prediction is subsequently introduced in Sec. 3.4, as illustrated in Fig. 2.

3.2. Textual-Aware Semantic Understanding

In this module, we build a textual semantic panorama that enables the agent to understand the environment from a textual perspective, allowing it to select the most relevant navigable view as the optimal local navigation action.

Salient Landmarks Extractor. The pretrained visual-language model readily provides the capability for agents to perceive textual semantics by generating detailed captions from RGB images. As illustrated in Fig. 2, we utilize off-the-shelf BLIP-2-FlanT5-xxL [29], a powerful visual-language model, to discretize R_t and generate corresponding textual descriptions for each view using the simple prompt “a photo of”. Following [15, 28], this process yields a textual panorama $\mathcal{S}_t = \{s_{t,i}\}_{i=1}^{n=36}$, where each view $s_{t,i}$ contains informed descriptions of salient landmarks. These descriptions typically involve room types and objects (e.g., “a living room with two chairs”), which assist in the object recognition. We further discuss the quality of the generated descriptions in supplementary materials. Additionally, we employ the CLIP (ViT-L-14-336px) text encoder [44] to extract textual semantic panorama features, embedding them as $\mathcal{X}_t^{\mathcal{S}} = \{x_{t,1}^s, \dots, x_{t,n}^s\}$. Thanks to the powerful yet frozen BLIP-2 and CLIP models, we empower the agent to obtain textual semantic features from the navigable nodes in its vicinity during navigation.

Textual Semantic Selector. Previous methods [31, 33, 50] aligned environmental RGB images with instructions by exploiting textual semantics yet the inherent modality discrepancy between visual and language modalities remained unaddressed. Similar to [39], we treat the textual semantic as a perceptual representation for navigation in this module, directly matching salient landmarks with the instructions. As shown in Fig. 2 and Fig. 3, our textual semantic selector combines both *static* and *dynamic* matching strategies to select the most instruction-relevant view in the textual panorama $\mathcal{X}_t^{\mathcal{S}}$.

Static Matching: The most straightforward approach to semantic alignment is by calculating similarity, where higher similarity indicates stronger relevance between the textual semantics of each view and the instruction. Consequently, we calculate the cosine similarity matrix $\mathbf{M} \in \mathbb{R}^{n \times l}$, which represents the correlation between each word in the instruction \mathcal{I} and each view in the textual panorama $\mathcal{X}_t^{\mathcal{S}}$. Nevertheless, the textual semantics generated only correspond to salient landmarks (e.g., “plant,” or “table”) rather than actions (e.g., “go to” or “turn left”) in the instructions. Therefore, we then apply row-wise max-pooling to purify the static instruction relevance $\Gamma_t^{stat} \in \mathbb{R}^n$ to match the most relevant landmarks between textual semantics and instructions at step t :

$$\mathbf{M}_{i,j} = \frac{\mathcal{X}_{t,i}^{\mathcal{S}} \cdot \mathcal{I}_j}{\|\mathcal{X}_{t,i}^{\mathcal{S}}\| \|\mathcal{I}_j\|}, \quad \Gamma_t^{stat} = \max_j \mathbf{M}_{i,j} \quad (1)$$

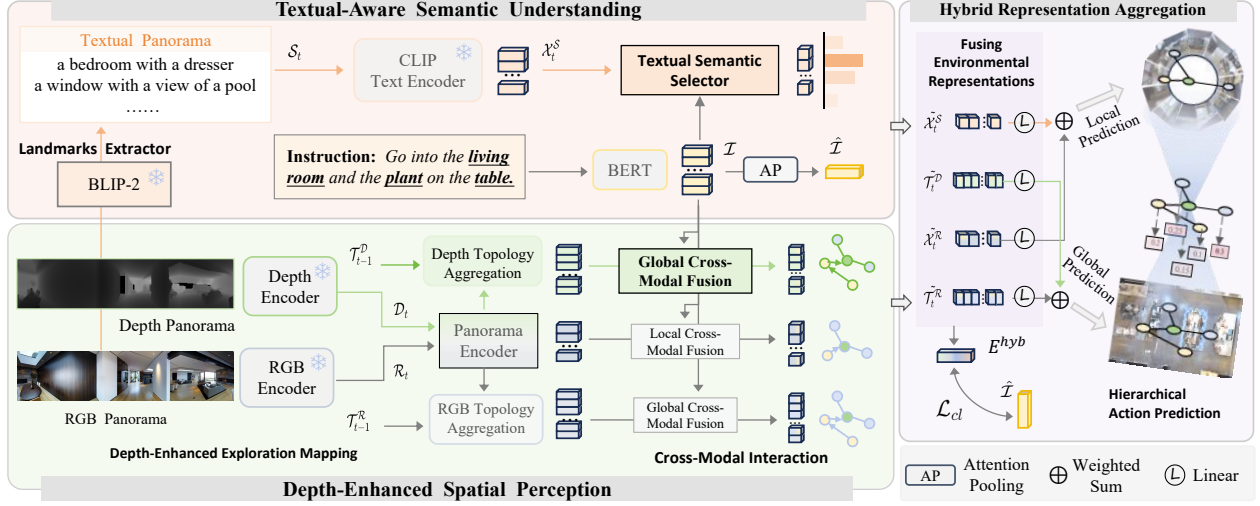


Figure 2. The detailed architecture of our proposed SUSA model. The orange and green arrows highlight our proposed Textual-Aware Semantic Understanding (TSU) and Depth-Aware Spatial Perception (DSP) modules, respectively. The Hybrid Representation Aggregation (HRA) module is designed for aligning environmental representations with instructions.

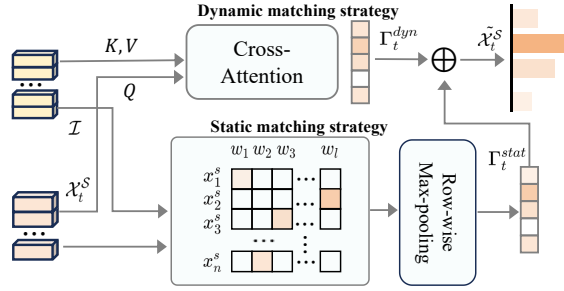


Figure 3. Illustration of TSU module in Fig. 2, which matches instructions and semantic features by static and dynamic strategies.

where $i = 1, \dots, n$ and $j = 1, \dots, l$. Although straightforward, the static strategy relies on the monotonic similarity matrix to match textual semantics \mathcal{X}_t^S and instructions \mathcal{I} , struggling with long-term navigation reasoning.

Dynamic Matching: Furthermore, a dynamic matching strategy is introduced to better capture the intricate relationships between the environment and instruction. Specifically, we utilize a standard multi-layer transformer decoder to dynamically match the relevance Γ_t^{dyn} between textual semantics and instructions, as formalized by:

$$\Gamma_t^{dyn} = \text{TCA}(\mathcal{X}_t^S, \mathcal{I}, \mathcal{I}), \quad (2)$$

where TCA denotes a **t**extual **m**odality **c**ross-**a**ttention mechanism that models textual semantic-instruction relationships. TCA comprises a cross-attention layer, a feed-forward network (FFN) layer, and LayerNorm, enabling the agent to adapt to long-term navigation sequences.

To trade off computational efficiency and navigation accuracy, we flexibly combine the relevance of static Γ_t^{sim} and

dynamic Γ_t^{att} . The latent semantic panoramic feature $\tilde{\mathcal{X}}_t^S$ is expressed as follows:

$$\tilde{\mathcal{X}}_t^S = \delta * \Gamma_t^{stat} + (1 - \delta) * \Gamma_t^{dyn}, \quad (3)$$

where the balance factor δ regulates the relative contributions of each matching strategy. By mapping the environment to the same textual modality, the textual semantic selector enables the agent to explicitly understand the environment context from a textual semantic perspective, thus facilitating grounded language instructions.

3.3. Depth-Enhanced Spatial Perception

Depth images, which also contain more intuitive and easily distinguishable structural information, were not adequately exploited in earlier works. To enhance the spatial perception, we concurrently construct a depth-based exploration map to memorize depth-based navigation trajectory alongside the RGB-based one [6].

Depth-Enhanced Exploration Mapping. Concretely, we obtain ground truth depth images for each view from the Matterport3D simulator. As illustrated in Fig. 2, we then employ ResNet-50 [17] (pretrained on the Gibson [57]) and CLIP (ViT-L/14@336px) as the depth and RGB encoders, respectively, to extract panoramic depth features $\mathcal{D}_t \in \mathbb{R}^{n \times d_v}$ and panoramic RGB features $\mathcal{R}_t \in \mathbb{R}^{n \times d_v}$, where d_v represents the dimension of each view. Moreover, we employ a two-layer transformer-based panorama encoding module to perform self-attention and sequentially encode the depth and RGB panoramic images. The panorama encoding modules for both modalities share weights, since each view in the depth and RGB panoramas is accordant.

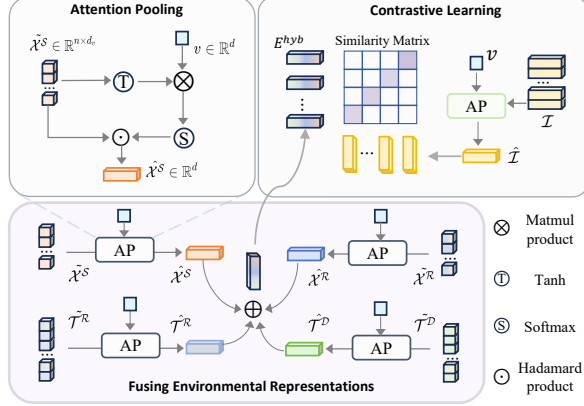


Figure 4. Illustration of the pipeline for fusing hybrid environmental representations in the proposed HRA module in Fig. 2.

Subsequently, we aggregate each visited node and its adjacent views by average pooling to construct depth and RGB exploration maps in parallel. The explored depth and RGB trajectory maps are formalized as $\mathcal{T}_t^D \in \mathbb{R}^{k \times d_n}$ and $\mathcal{T}_t^R \in \mathbb{R}^{k \times d_n}$. Here, k denotes the number of navigable nodes at step t , while d_n represents the dimension of each navigable node. These exploration maps memorize the agent navigation trajectory information for global action predictions, which serves to guide the agent traversal across various navigable nodes when considering backtracking.

Cross-Modal Interaction and Reasoning. To defer to instructions, we utilize a multi-layer cross-encoder that interacts with both the language instructions and the depth exploration map features to generate the refined depth map $\tilde{\mathcal{T}}^D$. This encoder comprises four residual connection layers of a cross-modal transformer, each incorporating graph-aware self-attention (GASA) [6], cross-modal attention, and a feed-forward network. The GASA operation is formally expressed as $\text{GASA}(X) = \tilde{\sigma}(X\Theta_q(X\Theta_k)^T + \mathcal{M})X\Theta_v$ where \mathcal{M} represents a learnable distance matrix encoding the relative distances between navigation nodes, $\tilde{\sigma}$ denotes the Softmax activation function, and $\Theta_q, \Theta_k, \Theta_v$ are learnable weight matrices. In parallel, we facilitate similar cross-modal interactions between the language instructions and the RGB exploration map \mathcal{T}^R , as well as the RGB panoramas \mathcal{X}^R . These are encoded as $\tilde{\mathcal{T}}^R$ and $\tilde{\mathcal{X}}^R$, thereby enabling the model to perform both global and local predictions based on the given instructions \mathcal{I} . Compared to the standalone \mathcal{T}^R , the incorporation of a depth exploration map \mathcal{T}^D enhances the perceptual clarity of environmental structures, mitigating the risk of overfitting to RGB-based visual noises [25] or biases [22, 51].

3.4. Hybrid Representation Aggregation

Building on aforementioned methods, at the current state t , the agent synchronously perceives the environment through

multiple modalities—textual semantic, depth, and RGB—at various scales (local and global). To encourage the agent to aggregate complementary context from these hybrid representations, we encode these features into a low-dimensional latent space via attention pooling and apply contrastive learning to align them with the instructions.

Fusing Hybrid Semantic-Spatial Environmental Representations. As depicted in Fig. 4, we employ attention pooling to project all environmental representations at time step t , along with the corresponding instruction, into an equivalent dimension d . Specifically, the attention pooling AP operation is defined as follows:

$$\hat{\mathcal{H}} = \text{AP}(\mathcal{H}, v), \quad \mathcal{H} \in \{\tilde{\mathcal{X}}^S, \tilde{\mathcal{T}}^D, \tilde{\mathcal{X}}^R, \tilde{\mathcal{T}}^R, \mathcal{I}\}, \quad (4)$$

where $v \in \mathbb{R}^d$ denoting the learnable query vector and $\hat{\mathcal{H}} \in \mathbb{R}^d$. The AP operator is given by:

$$\eta = \tilde{\sigma}(\tau(\mathcal{H}) \otimes v^T), \quad \hat{\mathcal{H}} = \tau(\eta \odot \mathcal{H}), \quad (5)$$

with τ representing the tanh activation function. Subsequently, we perform weighted aggregation of the hybrid environmental representations E^{hyb} , as follows:

$$\mathcal{B} = [\beta_1 \quad \beta_2 \quad \beta_3 \quad \beta_4]^T = \sigma(\text{FFN}[\tilde{\mathcal{X}}_0^S; \tilde{\mathcal{X}}_0^R; \tilde{\mathcal{T}}_0^D; \tilde{\mathcal{T}}_0^R]) \quad (6)$$

$$E^{\text{hyb}} = [\tilde{\mathcal{X}}^S \quad \tilde{\mathcal{X}}^R \quad \tilde{\mathcal{T}}^D \quad \tilde{\mathcal{T}}^R] \cdot \mathcal{B}, \quad (7)$$

where σ stands for the sigmoid activation function, and $[\cdot]$ denotes concatenation.

Hierarchical Action Prediction. We perform hierarchical action prediction by synergistically fusing the prediction scores from multiple branches to capture complementary information. Specifically, the scores for each branch are computed via separate FFN: $P_{\tilde{\mathcal{H}}} = \text{FFN}_{\tilde{\mathcal{H}}}(\tilde{\mathcal{H}})$, where $\tilde{\mathcal{H}} = \{x \in \mathcal{H} \mid x \neq \mathcal{I}\}$. Then, we apply weighted fusion to the textual semantic panorama \mathcal{X}^S and the RGB panorama \mathcal{X}^R to make local predictions, along with global predictions derived from exploration maps based on depth \mathcal{T}^D and RGB \mathcal{T}^R , which is formulated as:

$$P_{\mathcal{X}} = \beta_1 P_{\mathcal{X}^S} + \beta_2 P_{\mathcal{X}^R}, \quad (8)$$

$$P_{\mathcal{T}} = \beta_3 P_{\mathcal{T}^D} + \beta_4 P_{\mathcal{T}^R}. \quad (9)$$

We convert local predictions into the global action space and predict action a_t via dynamic fusing [6] $P_{\mathcal{T}}$ and $P_{\mathcal{X}}$.

3.5. Training and Inference

Pretraining. Our pre-training phase followed prior work [6, 30], utilizing auxiliary tasks such as Masked Language Modeling (MLM), Masked Region Classification (MRC), and Single-step Action Prediction (SAP). Object Grounding (OG) task to localize target objects in REVERIE and SOON. Given the sparsity of depth images and textual semantics compared to RGB images, completely pre-train all parameter of SUSA may lead to overfitting and increased training costs. As shown in Fig. 2, only the computation flows indicated by black arrows were pre-trained. The

effectiveness of this partial pre-trained strategy is demonstrated in Sec. 4.3.

Fine-tuning and Inference. During fine-tuning, we employ a contrastive learning loss, \mathcal{L}_{cl} to align the hybrid environmental representations E^{hyb} with the corresponding instructions \mathcal{I} :

$$\mathcal{L}_{cl} = -\frac{1}{2B} \sum_{i=1}^B \log \frac{\exp((E_i^{hyb}, \mathcal{I}_i)/t)}{\sum_{j=1}^B \exp((E_i^{hyb}, \mathcal{I}_j)/t)} - \frac{1}{2B} \sum_{i=1}^B \log \frac{\exp((\mathcal{I}_i, E_i^{hyb})/t)}{\sum_{j=1}^B \exp((\mathcal{I}_i, E_j^{hyb})/t)}, \quad (10)$$

where B and t represent the batch size and the temperature. Then, we train the model based on hybrid environment representations by performing single-step action prediction [5, 6] with a contrastive learning loss \mathcal{L}_{cl} . The hybrid single action prediction loss in behavior cloning is computed as $\mathcal{L}_{hsap}^{gt} = \sum_{t=1}^T -\log p(a_t^{gt} | \mathcal{I}, \mathcal{S}_t, \mathcal{D}_{<t}, \mathcal{R}_{<t})$ and $\mathcal{L}_{hsap}^* = \sum_{t=1}^T -\log p(a_t^* | \mathcal{I}, \mathcal{S}_t, \mathcal{D}_{<t}, \mathcal{R}_{<t})$, where a_t^{gt} represents the ground truth action, and a_t^* denotes the pseudo-target action sampled from current exploration map. The final training loss is then expressed as follows:

$$\mathcal{L}_{SUSA} = \lambda_1 \mathcal{L}_{hsap}^{gt} + \mathcal{L}_{hsap}^* + \lambda_2 \mathcal{L}_{cl} \quad (11)$$

where λ_1 and λ_2 denote loss weights.

During the inference phase, the agent is tasked with sequentially navigating to the predicted navigable nodes, following the shortest path algorithm [13], without making any abrupt ‘‘jumps’’ between nodes.

4. Experiments

4.1. Task Setup and Implementation

Datasets. We evaluate our model on three diverse VLN benchmarks based on the Matterport3D simulator environment [2]. **R2R** [2] focuses solely on navigation following detailed instructions. **REVERIE** [41] requires the agent to recognize the correct object from candidate bounding boxes upon reaching the navigation goal. **SOON** [64] further challenges agents to generate candidate bounding boxes using an object detector, as predefined boxes are not provided.

Metrics. We evaluate the navigation performance using standard metrics: Trajectory Length (TL), Success Rate (SR), Navigation Error (NE), and Success Rate weighted by Path Length (SPL). Additionally, we use Normalized Dynamic Time Warping (nDTW) and Success weighted by Normalized Dynamic Time Warping (sDTW) to evaluate the fidelity of successful trajectories to their corresponding instructions. For the REVERIE and SOON tasks, which involve object identification, we also evaluate object grounding metrics: Remote Grounding Success (RGS), and RGS weighted by Path Length (RGSPL). Given that SPL optimally balances navigation success rate and trajectory length, we employ it as our primary metric.

Implementation Details. We initialized transformer layers with pretrained LXMERT [48] during pre-training. Pre-training was performed for 100k iterations with a batch size of 32. Fine-tuning was performed for 25k iterations. For fine-tuning, we used batch sizes of 4, 8, and 2 for R2R, REVERIE, and SOON, respectively. The default hyperparameters are $\lambda_1 = 0.2$ and $\lambda_2 = 0.8$. The node and view dimensions are identical: $d_v = d_n = d = 768$. We minimized changes to the baseline (DUET) [6] settings and used no additional annotations. All experiments were conducted on a **single** NVIDIA RTX 4090 GPU. Detailed experimental setup is provided in the supplementary material.

4.2. Comparisons with State of the Art

We conduct a comprehensive comparison on the REVERIE [41], R2R [2], and SOON [64] datasets. For fairness, we exclude methods that involve pre-exploration [46, 66] or utilize large-scale data augmentation [7, 55]. **REVERIE.** Table 1 presents a comparative analysis on the REVERIE. On the test unseen split, SUSA achieves an SPL score of 41.54%, significantly outperforming the previous state-of-the-art (SOTA) method by a large margin of 2.78%. Furthermore, we establish new SOTA results for RGS and RGSPL on both the validation and test unseen splits, demonstrating that the introduced textual semantics substantially elevate overall navigation, particularly benefiting object localization performance. **R2R.** The compared experiment results on R2R, summarized in Tab. 2. Compared with the SOTA ESCENE [62] model on the validation and test unseen splits, SUSA achieves 64.85% and 63.83% on SPL, respectively. These gains manifest not only an improved navigation performance but also enhanced navigation efficiency, since SPL considers both success rate and trajectory length. **SOON.** On the SOON dataset, as shown in Tab. 3, SUSA achieves state-of-the-art performance across multiple metrics, including SR, SPL, and RGSPL, attaining SPL scores of 30.82% and 25.47% on the validation and test unseen splits, respectively. Moreover, SUSA consistently enhances the baseline (DUET)’s navigation performance and generalization on three datasets, underscoring the effectiveness of integrating textual semantics and depth exploration maps.

4.3. Diagnostic Experiment

1) Image Features vs. Structural Features. We analyze RGB and depth features contributions within the DSP module (Tab. 4). For RGB images, substituting ViT [11] features with those from CLIP [44] yields marked improvements across all metrics, highlighting that CLIP achieves a better understanding of the environment than its ViT-based baseline counterpart. As for depth features, we leveraged depth features extracted by ResNet-50 [17] pre-trained on the ImageNet [9] or Gibson [57] datasets to investigate the effect of depth exploration maps. Compared to ImageNet,

Methods	Validation Seen					Validation Unseen					Test Unseen				
	TL	SR \uparrow	SPL \uparrow	RGS \uparrow	RGSPL \uparrow	TL	SR \uparrow	SPL \uparrow	RGS \uparrow	RGSPL \uparrow	TL	SR \uparrow	SPL \uparrow	RGS \uparrow	RGSPL \uparrow
RCM [54]	10.70	23.33	21.82	16.23	15.36	11.98	9.29	6.97	4.89	3.89	10.60	7.84	6.67	3.67	3.14
HOP+ [43]	10.59	55.87	49.55	40.76	36.22	14.57	36.07	31.13	22.49	19.33	15.17	33.82	28.24	20.20	16.86
DSRG [50]	-	75.69	68.09	61.07	54.72	-	47.83	34.02	32.69	23.37	-	54.04	37.09	32.49	22.18
GridMM [56]	-	-	-	-	-	23.20	51.37	36.47	34.57	24.56	19.97	53.13	36.60	34.87	23.45
AZHP [58]	13.60	70.98	62.24	56.99	50.14	22.08	49.02	36.25	32.41	24.13	21.10	52.52	36.11	32.10	22.54
FDA [18]	-	-	-	-	-	19.04	47.57	35.90	32.06	24.31	17.30	49.62	36.45	30.34	22.08
CONSOLE [34]	-	74.14	65.15	60.08	52.69	-	50.07	34.40	34.05	23.33	-	55.13	37.13	33.18	22.25
KERM [31]	14.25	71.89	64.04	57.55	51.22	21.85	49.02	34.83	33.97	24.14	18.38	52.26	37.46	32.69	23.15
VER [36]	16.13	75.83	66.19	61.71	56.20	23.03	55.98	39.66	33.71	23.70	24.74	56.82	38.76	33.88	23.19
DUET [6]	13.86	71.75	63.94	57.41	51.14	22.11	46.98	33.73	32.15	23.03	21.30	52.51	36.06	31.88	22.06
SUSA (Ours)	14.60	76.95	69.07	61.77	55.86	22.59	51.75	38.86	35.02	26.56	17.86	54.39	41.54	36.11	27.31

Table 1. Comparison with the state of the art on REVERIE. **Bold** highlight the best performance in each column, \uparrow indicates better performance with higher values, ‘-’: unavailable statistics.

Methods	Validation Unseen				Test Unseen			
	TL	SR \uparrow	SPL \uparrow	NE \downarrow	TL	SR \uparrow	SPL \uparrow	NE \downarrow
RCM [54]	11.46	43	-	6.09	11.97	43	38	6.12
HOP [42]	12.27	64	57	3.80	12.68	64	59	3.83
DSRG [50]	-	73	62	<u>3.00</u>	-	72	61	3.33
PanoGen [28]	13.40	74	64	3.03	14.38	71	61	3.31
GridMM [56]	-	75	64	-	-	73	62	-
FDA [18]	13.68	72	64	3.41	14.76	69	62	3.41
KERM [31]	13.54	71.95	60.91	3.22	14.60	69.73	59.25	3.61
AZHP [58]	13.68	71	60	3.25	14.47	69	59	3.43
CONSOLE [34]	13.59	73	63	3.00	14.31	72	61	<u>3.30</u>
ESCENE [62]	10.80	68	<u>64</u>	3.39	11.89	66	<u>63</u>	3.77
DUET [6]	13.94	72	60	3.31	14.73	69	59	3.65
SUSA (Ours)	12.18	73.05	64.85	3.06	13.27	<u>72.56</u>	63.83	3.23

Table 2. Comparison with state of the art on the R2R dataset. **Bold** and Underline highlight the best and the runner-up performance in each column. \downarrow indicates better performance with lower values.* expressing our reimplement results.

Method	Validation Unseen				Test Unseen			
	TL	SR \uparrow	SPL \uparrow	RGSPL \uparrow	TL	SR \uparrow	SPL \uparrow	RGSPL \uparrow
GridMM [56]	38.92	37.46	24.81	3.91	46.20	36.27	21.25	4.15
SEAT [53]	-	36.87	24.87	3.91	-	35.89	22.55	4.47
KERM [31]	35.83	38.05	23.16	4.40	-	-	-	-
DUET [6]	36.20	36.28	22.58	3.75	41.83	33.44	21.42	4.17
SUSA(Ours)	36.86	42.89	30.82	6.48	36.13	36.87	25.47	5.93

Table 3. Comparison with the state of the art on the SOON.

the Gibson simulator provides spatial structural information that serves as valuable navigation priors. Therefore, in Tab. 4, the ResNet-50 pre-trained on the Gibson extracts structural features that refine spatial perception, yielding notable improvements in the SPL metric without compromising SR or RGS. These improvements indicate that better spatial perception enhances navigation efficiency.

2) Static Matching vs. Dynamic Matching. To assess the

RGB	Depth	OSR \uparrow	SR \uparrow	SPL \uparrow	RGS \uparrow	RGSPL \uparrow
ViT	<i>w/o</i>	51.07	46.98	33.73	32.15	23.03
CLIP	<i>w/o</i>	57.17	51.55	35.75	35.19	24.40
CLIP	ResNet-50(ImageNet)	54.42	50.18	34.63	34.39	23.66
CLIP	ResNet-50(Gibson)	56.72	52.00	39.21	35.05	26.54

Table 4. Ablation of different visual representations on the REVERIE validation unseen split. Gibson and ImageNet serve as pre-training sources for the depth encoder in the DSP module.

δ	REVERIE				R2R			
	SR \uparrow	SPL \uparrow	RGS \uparrow	RGSPL \uparrow	SR \uparrow	SPL \uparrow	nDTW \uparrow	sDTW \uparrow
<i>w/o</i>	52.00	39.21	35.05	26.54	72.80	62.71	69.33	60.21
0	53.91	38.87	36.84	26.82	72.20	63.78	70.74	61.46
0.5	55.07	39.50	37.12	26.70	73.05	64.85	71.05	62.17
1.0	53.51	37.86	36.69	25.92	72.37	62.95	69.17	60.55
<i>adaptive</i>	52.43	38.22	36.04	26.24	71.95	63.10	69.98	60.42

Table 5. Ablation on the relative importance of static and dynamic matching in the TSU module, balanced by the balance factor δ .

impact of static matching ($\delta = 0$) and dynamic matching ($\delta = 1$) strategies in the TSU module, we perform ablation studies based on balance factor δ on the R2R and REVERIE. Tab. 5 summarizes these results, where *w/o* indicates the exclusion of the TSU module, corresponding to the last row results in Tab. 4. Furthermore, *adaptive* denotes that δ is a learnable parameter which adaptively adjusts the contribution of each matching strategy. Compared to the first row in Tab. 5, overall, incorporating the TSU module (regardless of static or dynamic matching strategy) improves SR and RGS, albeit at the cost of SPL on REVERIE. In contrast, it enhances SPL on R2R. While the TSU module can achieve superior performance under the *adaptive* setting, its performance is inferior when $\delta = 0.5$. Specifically, at $\delta = 0.5$, the SPL metric reaches 39.50% and 64.85% on the two datasets, with the RGS, nDTW, and sDTW metrics also achieving optimal performance. Excellent results demonstrate dual merits of proposed TSU module, which boosts object identification accuracy on the REVERIE task

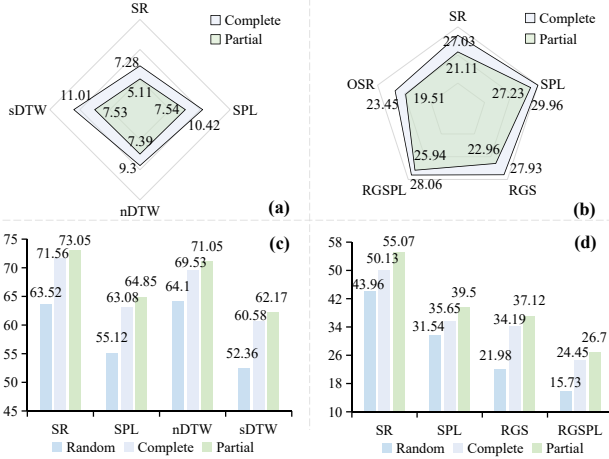


Figure 5. a) and b) show the performance gap (↓) between seen and unseen environments, while c) and d) present key metrics (↑) for different pretraining strategies on the R2R and REVERIE.

ID	DSP	TSU	HRA	SR	SPL	RGSPL
1	✗	✗	✗	46.98 52.51	33.73 36.06	23.03 22.06
2	✓	✗	✗	52.00 52.53	39.21 39.53	26.54 24.97
3	✗	✓	✗	53.17 53.89	38.31 40.89	26.73 26.43
4	✓	✓	✗	55.07 51.97	39.50 37.87	26.70 25.20
5	✓	✓	✓	51.75 54.39	38.86 41.54	26.56 27.31

Table 6. Ablation study on different components of SUSAs on the REVERIE (validation|test) unseen split.

while simultaneously improving the fidelity between navigation trajectories and instructions on the R2R.

3) Improved Generalization via Pretraining. As aforementioned in Sec. 3.5, pretraining the entire SUSAs framework on multiple auxiliary tasks may lead to overfitting, which may negatively impact the generalization in unseen environments, particularly considering the modality differences between textual panorama, depth exploration maps, and RGB representations. As shown in Fig. 5, we observe that the partial pretraining strategy not only consistently narrow the performance gap between seen and unseen environments but also outperform complete/random pretraining strategies in navigation performance. For example, as depicted in Fig. 5 (a), the partial pretraining model achieves an SR gap of only 21.11% between the seen and unseen splits on REVERIE, reducing the gap by 5.92% compared to the complete pretraining strategy. Additionally, as shown in Fig. 5 (c), multiple metrics indicate that partial pretraining results in superior performance. Fig. 5(b) and (d) illustrate similar trends are observed on R2R, further emphasizing the generalization of the partial pretraining strategy.

4) Overall Design. To thoroughly evaluate the efficacy of key components, we conduct ablation experiments on the REVERIE validation and test unseen split in the Tab. 6. As shown in Tab. 6, an intriguing phenomenon is observed: directly incorporating the DSP and TSU modules (#4) results

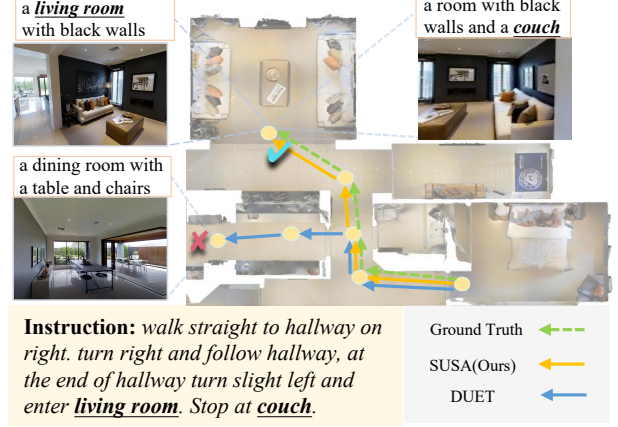


Figure 6. Predicted trajectories of SUSAs and DUET on the R2R validation unseen split.

in an improvement on validation unseen (e.g., SR=55.07, SPL=39.50), while performance on test unseen deteriorates. Conversely, contrastive learning within the HRA module (#5) produces opposite outcomes, particularly with respect to the SR metric. This may be attributed to the learnable token v , which, while pooling hybrid environmental representations, also introduces slight noise that causes fluctuations of navigation performance. Nevertheless, the overall performance is progressively improved with the inclusion of DSP, TSU and HRA modules. Analysis of the HRA module and the computational efficiency of the entire model is presented in supplementary materials.

4.4. Qualitative Analysis

As shown in Fig. 6, compared to DUET, our SUSAs agent is able to accurately stop near the “living room with a couch.” In contrast, the DUET agent, which relies exclusively on RGB environment representations, is prone to making elusive actions, hindering its ability to accurately follow instructions and reach the target location. This manifest that, thanks to the salient landmarks provided by the SUSAs architecture, the agent is better able to navigate to the target location by grounding textual instructions.

5. Conclusion

We present the SUSAs architecture, which exploits complementary semantic-spatial representations beyond RGB to facilitate environmental understanding and instruction grounding. Specifically, we propose the TSU module, enabling the agent to identify the most instruction-relevant semantic. The DSP module enhances spatial awareness by grounding depth exploration maps. We further employ contrastive learning to precisely align hybrid environmental representations with instructions. Experimental results on the R2R, REVERIE, and SOON benchmarks demonstrate the effectiveness and generalization of our approach. Future

work will enrich informative environmental representations to advance VLN tasks in continuous environments.

References

- [1] Dong An, Yuankai Qi, Yangguang Li, Yan Huang, Liang Wang, Tieniu Tan, and Jing Shao. Bevbort: Multimodal map pre-training for language-guided navigation. In *Proceedings of the IEEE/CVF International Conference on Computer Vision*, pages 2737–2748, 2023. 2, 3
- [2] Peter Anderson, Qi Wu, Damien Teney, Jake Bruce, Mark Johnson, Niko Sünderhauf, Ian Reid, Stephen Gould, and Anton Van Den Hengel. Vision-and-language navigation: Interpreting visually-grounded navigation instructions in real environments. In *Proceedings of the IEEE conference on computer vision and pattern recognition*, pages 3674–3683, 2018. 1, 2, 3, 6
- [3] Angel Chang, Angela Dai, Thomas Funkhouser, Maciej Halber, Matthias Niessner, Manolis Savva, Shuran Song, Andy Zeng, and Yinda Zhang. Matterport3d: Learning from RGB-D data in indoor environments. *International Conference on 3D Vision (3DV)*, 2017. 3
- [4] Peihao Chen, Dongyu Ji, Kunyang Lin, Runhao Zeng, Thomas Li, Mingkui Tan, and Chuang Gan. Weakly-supervised multi-granularity map learning for vision-and-language navigation. *Advances in Neural Information Processing Systems*, 35:38149–38161, 2022. 3
- [5] Shizhe Chen, Pierre-Louis Guhur, Cordelia Schmid, and Ivan Laptev. History aware multimodal transformer for vision-and-language navigation. *Advances in neural information processing systems*, 34:5834–5847, 2021. 1, 2, 6, 4
- [6] Shizhe Chen, Pierre-Louis Guhur, Makarand Tapaswi, Cordelia Schmid, and Ivan Laptev. Think global, act local: Dual-scale graph transformer for vision-and-language navigation. In *Proceedings of the IEEE/CVF Conference on Computer Vision and Pattern Recognition*, pages 16537–16547, 2022. 3, 4, 5, 6, 7, 1
- [7] Shizhe Chen, Pierre-Louis Guhur, Makarand Tapaswi, Cordelia Schmid, and Ivan Laptev. Learning from unlabeled 3d environments for vision-and-language navigation. In *European Conference on Computer Vision*, pages 638–655. Springer, 2022. 2, 6
- [8] Abhishek Das, Samyak Datta, Georgia Gkioxari, Stefan Lee, Devi Parikh, and Dhruv Batra. Embodied question answering. In *Proceedings of the IEEE Conference on Computer Vision and Pattern Recognition (CVPR)*, 2018. 1
- [9] Jia Deng, Wei Dong, Richard Socher, Li-Jia Li, Kai Li, and Li Fei-Fei. Imagenet: A large-scale hierarchical image database. In *2009 IEEE conference on computer vision and pattern recognition*, pages 248–255. Ieee, 2009. 6
- [10] Jacob Devlin, Ming-Wei Chang, Kenton Lee, and Kristina Toutanova. Bert: Pre-training of deep bidirectional transformers for language understanding. In *Proceedings of the 2019 conference of the North American chapter of the association for computational linguistics: human language technologies, volume 1 (long and short papers)*, pages 4171–4186, 2019. 3
- [11] Alexey Dosovitskiy, Lucas Beyer, Alexander Kolesnikov, Dirk Weissenborn, Xiaohua Zhai, Thomas Unterthiner, Mostafa Dehghani, Matthias Minderer, Georg Heigold, Sylvain Gelly, et al. An image is worth 16x16 words: Transformers for image recognition at scale. In *International Conference on Learning Representations*, 2020. 6
- [12] Mengfei Du, Binhao Wu, Jiwen Zhang, Zhihao Fan, Zejun Li, Ruipu Luo, Xuan-Jing Huang, and Zhongyu Wei. Delan: Dual-level alignment for vision-and-language navigation by cross-modal contrastive learning. In *Proceedings of the 2024 Joint International Conference on Computational Linguistics, Language Resources and Evaluation (LREC-COLING 2024)*, pages 4605–4616, 2024. 1, 2
- [13] Robert W Floyd. Algorithm 97: shortest path. *Communications of the ACM*, 5(6):345–345, 1962. 6
- [14] Daniel Fried, Ronghang Hu, Volkan Cirik, Anna Rohrbach, Jacob Andreas, Louis-Philippe Morency, Taylor Berg-Kirkpatrick, Kate Saenko, Dan Klein, and Trevor Darrell. Speaker-follower models for vision-and-language navigation. *Advances in Neural Information Processing Systems*, 31, 2018. 2
- [15] Fang Gao, Jingfeng Tang, Jiabao Wang, Shaocong Li, and Jun Yu. Enhancing scene understanding for vision-and-language navigation by knowledge awareness. *IEEE Robotics and Automation Letters*, 2024. 3, 2
- [16] Georgios Georgakis, Karl Schmeckpeper, Karan Wanchoo, Soham Dan, Eleni Miltsakaki, Dan Roth, and Kostas Daniilidis. Cross-modal map learning for vision and language navigation. In *Proceedings of the IEEE/CVF Conference on Computer Vision and Pattern Recognition*, pages 15460–15470, 2022. 2
- [17] Kaiming He, Xiangyu Zhang, Shaoqing Ren, and Jian Sun. Deep residual learning for image recognition. In *Proceedings of the IEEE conference on computer vision and pattern recognition*, pages 770–778, 2016. 4, 6
- [18] Keji He, Chenyang Si, Zhihe Lu, Yan Huang, Liang Wang, and Xinchao Wang. Frequency-enhanced data augmentation for vision-and-language navigation. *Advances in Neural Information Processing Systems*, 36, 2024. 2, 3, 7
- [19] Haodong Hong, Yanyuan Qiao, Sen Wang, Jiajun Liu, and Qi Wu. General scene adaptation for vision-and-language navigation. *arXiv preprint arXiv:2501.17403*, 2025. 3
- [20] Yicong Hong, Qi Wu, Yuankai Qi, Cristian Rodriguez-Opazo, and Stephen Gould. Vln bert: A recurrent vision-and-language bert for navigation. In *Proceedings of the IEEE/CVF conference on Computer Vision and Pattern Recognition*, pages 1643–1653, 2021. 1, 2
- [21] Yicong Hong, Yang Zhou, Ruiyi Zhang, Franck Dernoncourt, Trung Bui, Stephen Gould, and Hao Tan. Learning navigational visual representations with semantic map supervision. In *Proceedings of the IEEE/CVF International Conference on Computer Vision*, pages 3055–3067, 2023. 3
- [22] Ronghang Hu, Daniel Fried, Anna Rohrbach, Dan Klein, Trevor Darrell, and Kate Saenko. Are you looking? grounding to multiple modalities in vision-and-language navigation. In *Proceedings of the 57th Annual Meeting of the Association for Computational Linguistics*, pages 6551–6557, 2019. 2, 5

- [23] Chenguang Huang, Oier Mees, Andy Zeng, and Wolfram Burgard. Visual language maps for robot navigation. In *2023 IEEE International Conference on Robotics and Automation (ICRA)*, pages 10608–10615. IEEE, 2023. 2
- [24] Minyoung Hwang, Jaeyeon Jeong, Minsoo Kim, Yoonseon Oh, and Songhwai Oh. Meta-explore: Exploratory hierarchical vision-and-language navigation using scene object spectrum grounding. In *Proceedings of the IEEE/CVF Conference on Computer Vision and Pattern Recognition*, pages 6683–6693, 2023. 3
- [25] Nikolai Ilinykh, Yasmeen Emampoor, and Simon Dobnik. Look and answer the question: On the role of vision in embodied question answering. In *Proceedings of the 15th International Conference on Natural Language Generation*, pages 236–245, 2022. 5
- [26] Liyiming Ke, Xiujun Li, Yonatan Bisk, Ari Holtzman, Zhe Gan, Jingjing Liu, Jianfeng Gao, Yejin Choi, and Siddhartha Srinivasa. Tactical rewind: Self-correction via backtracking in vision-and-language navigation. In *Proceedings of the IEEE/CVF conference on computer vision and pattern recognition*, pages 6741–6749, 2019. 2
- [27] Alexander Ku, Peter Anderson, Roma Patel, Eugene Ie, and Jason Baldridge. Room-Across-Room: Multilingual vision-and-language navigation with dense spatiotemporal grounding. In *Conference on Empirical Methods for Natural Language Processing (EMNLP)*, 2020. 1
- [28] Jialu Li and Mohit Bansal. Panogen: Text-conditioned panoramic environment generation for vision-and-language navigation. *Advances in Neural Information Processing Systems*, 36:21878–21894, 2023. 3, 7
- [29] Junnan Li, Dongxu Li, Silvio Savarese, and Steven Hoi. Blip-2: Bootstrapping language-image pre-training with frozen image encoders and large language models. In *International conference on machine learning*, pages 19730–19742. PMLR, 2023. 1, 3
- [30] Mingxiao Li, Zehao Wang, Tinne Tuytelaars, and Marie-Francine Moens. Layout-aware dreamer for embodied visual referring expression grounding. In *Proceedings of the AAAI Conference on Artificial Intelligence*, pages 1386–1395, 2023. 3, 5, 1
- [31] Xiangyang Li, Zihan Wang, Jiahao Yang, Yaowei Wang, and Shuqiang Jiang. Kerm: Knowledge enhanced reasoning for vision-and-language navigation. In *Proceedings of the IEEE/CVF Conference on Computer Vision and Pattern Recognition*, pages 2583–2592, 2023. 1, 2, 3, 7
- [32] Xiwen Liang, Fengda Zhu, Yi Zhu, Bingqian Lin, Bing Wang, and Xiaodan Liang. Contrastive instruction-trajectory learning for vision-language navigation. In *Proceedings of the AAAI Conference on Artificial Intelligence*, pages 1592–1600, 2022. 1, 2
- [33] Bingqian Lin, Yi Zhu, Xiaodan Liang, Liang Lin, and Jianzhuang Liu. Actional atomic-concept learning for demystifying vision-language navigation. In *Proceedings of the AAAI Conference on Artificial Intelligence*, pages 1568–1576, 2023. 1, 2, 3
- [34] Bingqian Lin, Yunshuang Nie, Ziming Wei, Yi Zhu, Hang Xu, Shikui Ma, Jianzhuang Liu, and Xiaodan Liang. Correctable landmark discovery via large models for vision-language navigation. *IEEE Transactions on Pattern Analysis and Machine Intelligence*, 2024. 1, 2, 7
- [35] Chong Liu, Fengda Zhu, Xiaojun Chang, Xiaodan Liang, Zongyuan Ge, and Yi-Dong Shen. Vision-language navigation with random environmental mixup. In *Proceedings of the IEEE/CVF International Conference on Computer Vision*, pages 1644–1654, 2021. 3
- [36] Rui Liu, Wenguan Wang, and Yi Yang. Volumetric environment representation for vision-language navigation. In *Proceedings of the IEEE/CVF Conference on Computer Vision and Pattern Recognition*, pages 16317–16328, 2024. 2, 3, 7
- [37] Shubo Liu, Hongsheng Zhang, Yuankai Qi, Peng Wang, Yan-ni Zhang, and Qi Wu. Aerialvln: Vision-and-language navigation for uavs. In *Proceedings of the IEEE/CVF International Conference on Computer Vision*, pages 15384–15394, 2023. 1
- [38] Aly Magassouba, Komei Sugiura, and Hisashi Kawai. Crossmap transformer: A crossmodal masked path transformer using double back-translation for vision-and-language navigation. *IEEE Robotics and Automation Letters*, 6(4):6258–6265, 2021. 1, 2
- [39] Bowen Pan, Rameswar Panda, SouYoung Jin, Rogerio Feris, Aude Oliva, Phillip Isola, and Yoon Kim. Langnav: Language as a perceptual representation for navigation. In *Findings of the Association for Computational Linguistics: NAACL 2024*, pages 950–974, 2024. 3
- [40] Alexander Pashevich, Cordelia Schmid, and Chen Sun. Episodic transformer for vision-and-language navigation. In *Proceedings of the IEEE/CVF International Conference on Computer Vision*, pages 15942–15952, 2021. 1, 2
- [41] Yuankai Qi, Qi Wu, Peter Anderson, Xin Wang, William Yang Wang, Chunhua Shen, and Anton van den Hengel. Reverie: Remote embodied visual referring expression in real indoor environments. In *Proceedings of the IEEE/CVF Conference on Computer Vision and Pattern Recognition*, pages 9982–9991, 2020. 1, 2, 3, 6
- [42] Yanyuan Qiao, Yuankai Qi, Yicong Hong, Zheng Yu, Peng Wang, and Qi Wu. Hop: History-and-order aware pre-training for vision-and-language navigation. In *Proceedings of the IEEE/CVF Conference on Computer Vision and Pattern Recognition*, pages 15418–15427, 2022. 7
- [43] Yanyuan Qiao, Yuankai Qi, Yicong Hong, Zheng Yu, Peng Wang, and Qi Wu. Hop+: History-enhanced and order-aware pre-training for vision-and-language navigation. *IEEE Transactions on Pattern Analysis and Machine Intelligence*, 2023. 7
- [44] Alec Radford, Jong Wook Kim, Chris Hallacy, Aditya Ramesh, Gabriel Goh, Sandhini Agarwal, Girish Sastry, Amanda Askell, Pamela Mishkin, Jack Clark, et al. Learning transferable visual models from natural language supervision. In *International conference on machine learning*, pages 8748–8763. PMLR, 2021. 1, 2, 3, 6
- [45] Mohit Shridhar, Jesse Thomason, Daniel Gordon, Yonatan Bisk, Winson Han, Roozbeh Mottaghi, Luke Zettlemoyer, and Dieter Fox. Alfred: A benchmark for interpreting grounded instructions for everyday tasks. In *Proceedings of*

- the *IEEE/CVF conference on computer vision and pattern recognition*, pages 10740–10749, 2020. 1
- [46] Gunnar A Sigurdsson, Jesse Thomason, Gaurav S Sukhatme, and Robinson Piramuthu. Rrex-bot: Remote referring expressions with a bag of tricks. In *2023 IEEE/RSJ International Conference on Intelligent Robots and Systems (IROS)*, pages 5203–5210. IEEE, 2023. 6
- [47] Xue Song, Jiequan Cui, Hanwang Zhang, Jingjing Chen, Richang Hong, and Yu-Gang Jiang. Doubly abductive counterfactual inference for text-based image editing. In *Proceedings of the IEEE/CVF Conference on Computer Vision and Pattern Recognition*, pages 9162–9171, 2024. 1
- [48] Hao Tan and Mohit Bansal. Lxmert: Learning cross-modality encoder representations from transformers. In *Proceedings of the 2019 Conference on Empirical Methods in Natural Language Processing and the 9th International Joint Conference on Natural Language Processing (EMNLP-IJCNLP)*, pages 5100–5111, 2019. 6
- [49] Sinan Tan, Mengmeng Ge, Di Guo, Huaping Liu, and Fuchun Sun. Depth-aware vision-and-language navigation using scene query attention network. In *2022 International Conference on Robotics and Automation (ICRA)*, pages 9390–9396. IEEE, 2022. 2, 3
- [50] Liuyi Wang, Zongtao He, Jiagui Tang, Ronghao Dang, Naijia Wang, Chengju Liu, and Qijun Chen. A dual semantic-aware recurrent global-adaptive network for vision-and-language navigation. In *Proceedings of the Thirty-Second International Joint Conference on Artificial Intelligence*, pages 1479–1487, 2023. 1, 3, 7, 4
- [51] Liuyi Wang, Zongtao He, Ronghao Dang, Mengjiao Shen, Chengju Liu, and Qijun Chen. Vision-and-language navigation via causal learning. In *Proceedings of the IEEE/CVF Conference on Computer Vision and Pattern Recognition*, pages 13139–13150, 2024. 2, 5
- [52] Liuyi Wang, Chengju Liu, Zongtao He, Shu Li, Qingqing Yan, Huiyi Chen, and Qijun Chen. Pasts: Progress-aware spatio-temporal transformer speaker for vision-and-language navigation. *Engineering Applications of Artificial Intelligence*, 128:107487, 2024. 1, 2
- [53] Liuyi Wang, Jiagui Tang, Zongtao He, Ronghao Dang, Chengju Liu, and Qijun Chen. Enhanced language-guided robot navigation with panoramic semantic depth perception and cross-modal fusion. In *2024 IEEE/RSJ International Conference on Intelligent Robots and Systems (IROS)*, pages 7726–7733. IEEE, 2024. 2, 3, 7
- [54] Xin Wang, Qiuyuan Huang, Asli Celikyilmaz, Jianfeng Gao, Dinghan Shen, Yuan-Fang Wang, William Yang Wang, and Lei Zhang. Reinforced cross-modal matching and self-supervised imitation learning for vision-language navigation. In *Proceedings of the IEEE/CVF conference on computer vision and pattern recognition*, pages 6629–6638, 2019. 2, 7
- [55] Zun Wang, Jialu Li, Yicong Hong, Yi Wang, Qi Wu, Mohit Bansal, Stephen Gould, Hao Tan, and Yu Qiao. Scaling data generation in vision-and-language navigation. In *Proceedings of the IEEE/CVF International Conference on Computer Vision*, pages 12009–12020, 2023. 2, 3, 6
- [56] Zihan Wang, Xiangyang Li, Jiahao Yang, Yeqi Liu, and Shuqiang Jiang. Gridmm: Grid memory map for vision-and-language navigation. In *Proceedings of the IEEE/CVF International Conference on Computer Vision*, pages 15625–15636, 2023. 2, 3, 7
- [57] Fei Xia, Amir R Zamir, Zhiyang He, Alexander Sax, Jitendra Malik, and Silvio Savarese. Gibson env: Real-world perception for embodied agents. In *Proceedings of the IEEE conference on computer vision and pattern recognition*, pages 9068–9079, 2018. 4, 6
- [58] Zhaohuan Zhan, Jinghui Qin, Wei Zhuo, and Guang Tan. Enhancing vision and language navigation with prompt-based scene knowledge. *IEEE Transactions on Circuits and Systems for Video Technology*, 2024. 7
- [59] Xuesong Zhang, Jun He, Jia Zhao, Zhenzhen Hu, Xun Yang, Jia Li, and Richang Hong. Exploring and exploiting model uncertainty for robust visual question answering. *Multimedia Systems*, 30(6):1–14, 2024. 1
- [60] Xuesong Zhang, Jia Li, Yunbo Xu, Zhenzhen Hu, and Richang Hong. Seeing is believing? enhancing vision-language navigation using visual perturbations. *arXiv preprint arXiv:2409.05552*, 2024. 3
- [61] Yubo Zhang, Hao Tan, and Mohit Bansal. Diagnosing the environment bias in vision-and-language navigation. In *Proceedings of the Twenty-Ninth International Conference on International Joint Conferences on Artificial Intelligence*, pages 890–897, 2021. 2
- [62] Qi Zheng, Daqing Liu, Chaoyue Wang, Jing Zhang, Dadong Wang, and Dacheng Tao. Esceme: Vision-and-language navigation with episodic scene memory. *International Journal of Computer Vision*, pages 1–21, 2024. 6, 7
- [63] Fengda Zhu, Yi Zhu, Xiaojun Chang, and Xiaodan Liang. Vision-language navigation with self-supervised auxiliary reasoning tasks. In *Proceedings of the IEEE/CVF conference on computer vision and pattern recognition*, pages 10012–10022, 2020. 2
- [64] Fengda Zhu, Xiwen Liang, Yi Zhu, Qizhi Yu, Xiaojun Chang, and Xiaodan Liang. Soon: Scenario oriented object navigation with graph-based exploration. In *Proceedings of the IEEE/CVF Conference on Computer Vision and Pattern Recognition*, pages 12689–12699, 2021. 1, 2, 3, 6
- [65] Wanrong Zhu, Yuankai Qi, Pradyumna Narayana, Kazuo Sone, Sugato Basu, Eric Xin Wang, Qi Wu, Miguel Eckstein, and William Yang Wang. Diagnosing vision-and-language navigation: what really matters. In *2022 Conference of the North American Chapter of the Association for Computational Linguistics: Human Language Technologies, NAACL 2022*, pages 5981–5993. Association for Computational Linguistics (ACL), 2022. 2
- [66] Yi Zhu, Fengda Zhu, Zhaohuan Zhan, Bingqian Lin, Jianbin Jiao, Xiaojun Chang, and Xiaodan Liang. Vision-dialog navigation by exploring cross-modal memory. In *Proceedings of the IEEE/CVF Conference on Computer Vision and Pattern Recognition*, pages 10730–10739, 2020. 2, 6
- [67] Daoming Zong, Chaoyue Ding, Baoxiang Li, Jiakui Li, and Ken Zheng. Balancing multimodal learning via online logit modulation. In *Proceedings of the Thirty-Third International Joint Conference on Artificial Intelligence*, pages 5753–5761, 2024. 2

Agent Journey Beyond RGB: Unveiling Hybrid Semantic-Spatial Environmental Representations for Vision-and-Language Navigation

Supplementary Material

6. Detailed Experimental Setups

Metrics. We categorize the metrics into three types: *Navigation*, *Objects Grounding*, and *Instruction Following*. Detailed calculations of these metrics can be found in Tab. 7. For *Navigation* metrics, Trajectory Length (TL): Average path length in meters. It is worth noting that since the trajectory needs to match the ground truth trajectory described by the instruction, strictly speaking, the trajectory length is not necessarily the smaller, the better. Success Rate (SR): Proportion of paths where the agent reaches within 3 meters of the target location. Oracle Success Rate (OSR): The proportion of trajectories where at least one node is within 3 meters of a corresponding node in the reference trajectory. Navigation Error (NE): Average final distance (meters) between the agent and the target. Success Rate weighted by Path Length (SPL): Prioritizes success for shorter paths, which normalizes the success rate by trajectory length. For *Instruction Following* metrics, we apply Normalized Dynamic Time Warping (nDTW) and Success Rate Weighted by Dynamic Time Warping (sDTW). The former measures how well the VLN agent could follow the instruction, while the latter considers nDTW for success cases. For *Objects Grounding* metrics: Remote Grounding Success (RGS): Proportion of instructions where the agent correctly identifies the target object. RGS weighted by Path Length (RGSPL): Prioritizes correct object identification for shorter paths.

Pre-training Tasks. Following prior works [5, 6, 30], during pre-training, we employ a suite of multimodal pre-training tasks, including MLM (Masked Language Modeling), MRC (Masked Region Classification), SAP (Single Action Prediction), and OG (Object Grounding). OG is specifically designed for object grounding using the REVERIE and SOON datasets. MLM and MRC aim to establish a robust vision-language alignment. SAP enables the agent to learn preliminary navigation knowledge by predicting the next action during pre-training. However, as navigation is inherently a sequential decision-making process, SAP can only learn static, single-step decisions.

Dataset Details. We evaluate the navigation capabilities of the agent on three distinct VLN datasets: the fine-grained R2R [2], as well as the goal-oriented REVERIE [41] and SOON [64] datasets, as shown in Tab. 8. Each dataset is divided into train, validation seen, validation unseen, and test unseen splits. REVERIE contains approximately 20k high-level instructions describing target locations and ob-

Metric	↑↓	Definition	Dataset
Navigation:			
TL		$\sum_{1 \leq i < P } d(p_i, p_{i+1})$	R2R REVERIE SOON
NE	↓	$d(p_{ P }, g_{ G })$	
ONE	↓	$\min_{p \in P} d(p, g_{ G })$	
SR	↑	$\mathbb{I}[NE(P, G) \leq d_{th}]$	
OSR	↑	$\mathbb{I}[\text{ONE}(P, G) \leq d_{th}]$	
SPL	↑	$\text{SR}(P, G) \cdot \frac{d(p_1, g_{ G })}{\max\{\text{TL}(P), d(p_1, g_{ G })\}}$	
Instruction Following:			
nDTW	↑	$\exp\left(-\frac{\min_{w \in \mathcal{W}} \sum_{(i_k, j_k) \in w} d(p_{i_k}, q_{j_k})}{ P \cdot d_{th}}\right)$	R2R
sDTW	↑	$\text{SR}(P, G) * \text{nDTW}(P, G)$	
Objects Grounding:			
RGS	↑	$\mathbb{I}\left(\max_j \text{IoU}(B_i^p, B_j^g) \geq 0.5\right)$	REVERIE SOON
RGSPL	↑	$\text{RGS}(P, G) \cdot \frac{d(p_1, g_{ G })}{\max\{\text{TL}(P), d(p_1, g_{ G })\}}$	

Table 7. Common VLN metrics, categorized into three types: Navigation, Instruction Following, and Object Grounding. The symbols ↑ and ↓ signify if a higher or lower metric value is preferable, respectively. P represents the paths taken by the agent, while G stands for the ground truth trajectories. The function $\mathbb{I}(\cdot)$ serves as an indicator, with $d(n, P)$ measuring the distance from node n to path P , and d_{th} indicating the distance threshold. $W = w_{1..|W|}$ is a warping with $w_k = (i_k, j_k) \in [1 : |P|], [1 : |G|]$, respecting the step-size. B_i^p means the i -th object’s bounding box in agent path (or trajectory).

jects, with an average instruction length of 21 words. Given predefined object bounding boxes within each panorama, the agent identifies the correct bounding box upon reaching the navigation goal. Unlike the R2R dataset, in the REVERIE task, the agent must identify the correct bounding box from the candidates once the navigation target is reached. R2R includes 22k step-by-step instructions, with an average instruction length of 32 words. The R2R dataset focuses solely on the navigation task, providing detailed path planning for the agent in the instructions. SOON is another goal-oriented dataset, containing about 5k instructions, each averaging 47 words in length.

We evaluated the experimental results of the unseen test split on the public online leaderboards¹. We assure the readers that we will make our code and model checkpoints publicly available.

¹<https://eval.ai/web/challenges/challenge-page/606/participate>,
<https://eval.ai/web/challenges/challenge-page/97/participate>

Dataset	Train		Validation Seen		Validation Unseen		Test Unseen		VLN task
	instr	house	instr	house	instr	house	instr	house	
R2R [2]	14039	61	1021	56	2349	11	4173	18	Fine-grained
REVERIE [41]	10466	60	1423	46	3521	10	6292	16	Goal-oriented
SOON [64]	2779	34	113	2	339	5	615	14	Goal-oriented

Table 8. Comparison of the three VLN datasets utilized in this study.

Methods		Validation Unseen				
		TL	SR	SPL	RGS	RGSPL
Depth	BEVBert [1]	-	51.78	36.37	34.71	24.44
	GridMM [56]	23.20	51.37	36.47	34.57	24.56
	SEAT[53]	-	49.45	35.51	32.83	23.14
	SUSA(DP)	24.43	52.54	37.59	35.47	25.27
	SUSA(DEM)	22.88	52.00	39.21	35.05	26.54
Text	KESU [15]	22.93	50.36	35.15	35.02	24.17
	KERM [31]	21.85	50.44	35.38	34.51	24.45
	AACL [33]	22.11	49.42	33.54	33.31	22.49
	CONSOLE [34]	-	50.07	34.40	34.05	23.33
	SUSA(TP)	23.40	53.17	38.31	37.18	26.73

Table 9. Comparison with related works on the REVERIE validation unseen split.

7. Additional Experiments

7.1. Comparison with Previous Approaches

We demonstrate the effectiveness of the proposed method through comparisons with related approaches. As shown in Tab. 9, experiments reveal that directly grounding depth information—whether using depth panoramas (DP) or depth exploration maps (DEM) as input—outperforms prior depth-based methods [1, 53, 56]. Notably, using depth exploration maps leads to better navigation performance than depth panoramas. Similarly, directly aligning textual semantics with instructions via textual panoramas (TP) surpasses methods [15, 31, 34] that integrate textual semantics into environmental representations. This underscores the superiority of independently grounding each modality, improving the interpretability of each modality’s contribution.

7.2. Fusion Weights of Hybrid Representations.

We quantitatively illustrate the weights (see Eq. (6)) assigned to each branch of the HRA module during training (in Fig. 7) and inference (in Tab. 10). These weights are normalized between 0 and 1, with higher values denoting stronger dependency on the corresponding environmental representation. As shown in Fig. 7, initially, all four representations have approximately equal weights of 0.25 during training, reflecting random initialization and balanced contributions. Over the course of training, the global RGB representation weight β_4 increases, while those of the textual semantic β_1 and depth β_3 modalities decrease. This trend arises because textual semantics and depth provide sparse

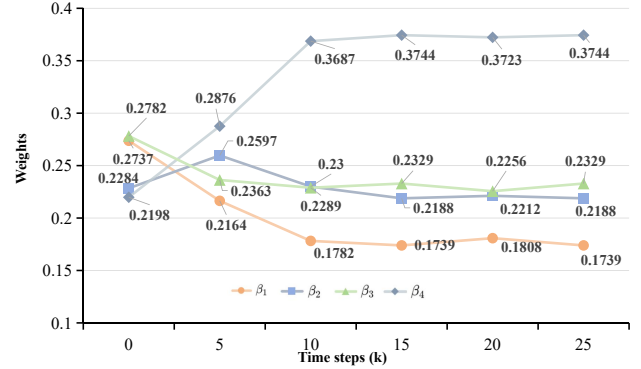


Figure 7. The weights for hybrid representations in the HRA module change during training (see Eq. (6)).

Splits	Local		Global	
	Semantic β_1	RGB β_2	Depth β_3	RGB β_4
Validation Seen	0.2147	0.2458	0.2239	0.3156
Validation Unseen	0.2151	0.2662	0.2216	0.2971

Table 10. Variation in fusion weights (in Eq. (6)) of hybrid representations during inference on R2R. $\beta_1, \beta_2, \beta_3, \beta_4$ denotes the fusion weight of textual semantic, local RGB, depth, global RGB representations in the HRA module, respectively.

yet precise information, which is particularly beneficial in the early stages of training. Despite the increasing dominance of the RGB modality, the agent’s reliance on textual semantics and depth remains above 20%, underscoring their essential role in navigation. Tab. 10 also demonstrates that the agent effectively utilizes the introduced depth spatial and textual semantic information during inference, even though it exhibits a stronger reliance on the RGB modality.

7.3. Quality of Generated Salient Landmarks

The quality of the extracted salient landmarks is crucial for the agent to accurately understand the textual semantics of the environment. In Fig. 8, we compute the similarity between the top-50 most frequently occurring landmarks in our generated salient landmarks and those from R2R [2] and REVERIE [41] to evaluate the quality of the generated salient landmarks. While the types and frequencies of these generated landmarks is different from those in the datasets, they can contain and convey most similar semantic (similar-

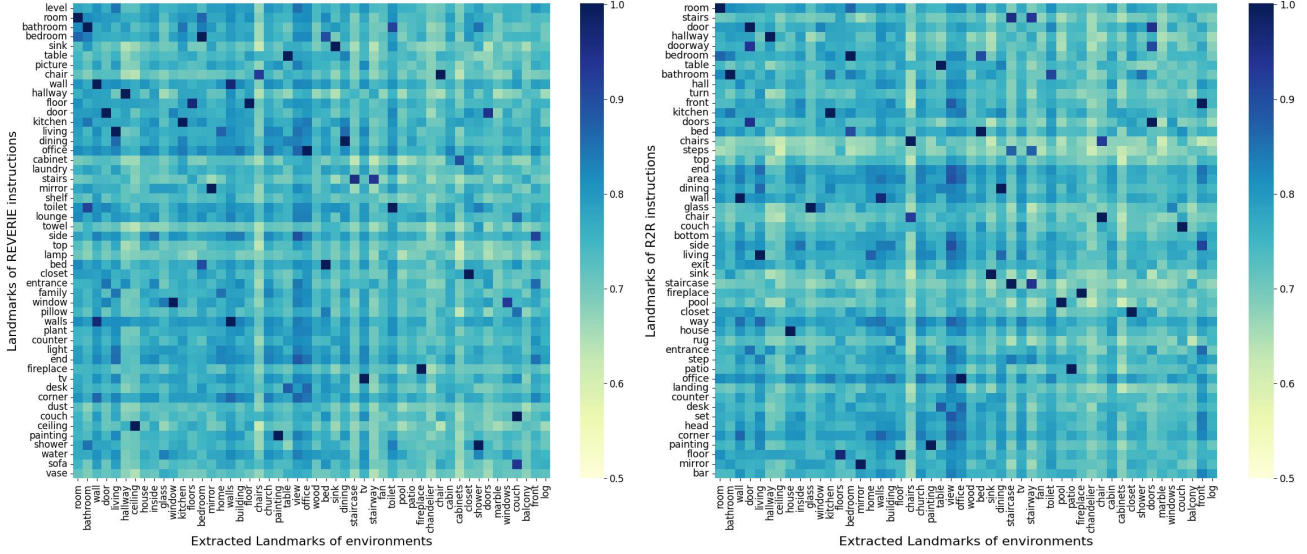


Figure 8. Similarity matrix for the top 50 most frequent landmarks: REVERIE instructions vs. environments (left), R2R instructions vs. environments (right). Best viewed in color.

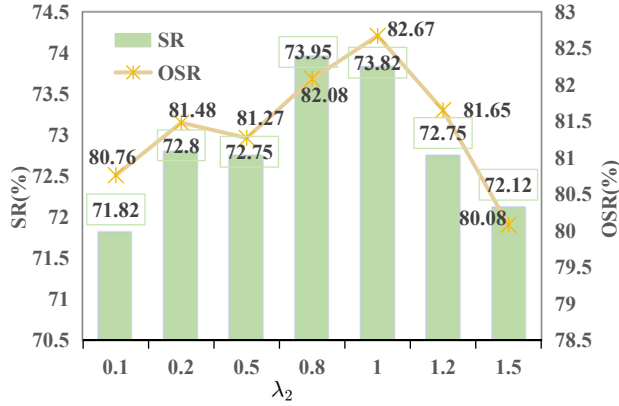


Figure 9. Analysis of the contrastive loss weight λ_2 in HRA module on R2R validation unseen split.

ities surpass 0.5). Notably, the plug-and-play CLIP text encoder excels in understanding image-related descriptions, while BERT is more adept at comprehending natural language sentences. Therefore, we use the CLIP text encoder to extract features from the generated salient landmarks.

7.4. Analysis of the Contrastive Loss Weight

Our ablation studies indicate that the contrastive learning loss weight, denoted as λ_2 in Eq. (11), affects model navigation performance. As shown in Fig. 9, agent achieves the optimal navigation performance when the λ_2 is set to 0.8. we further observe that, within a certain range, increasing the contrastive loss weight improves navigation performance. However, when the contrastive loss weight is too

ID	DSP	TSU	HRA	TL	NE↓	OSR↑	SR↑	SPL↑
1	✗	✗	✗	13.41	3.30	79.86	71.43	60.63
2	✓	✗	✗	13.85	3.08	80.42	72.80	62.71
3	✗	✓	✗	13.78	3.06	81.65	72.92	63.16
4	✓	✓	✗	12.18	3.06	79.99	73.05	64.85
5	✓	✓	✓	14.58	3.08	82.08	73.95	62.84

Table 11. Ablation study on different components of SUSA on the R2R validation unseen split.

high, performance (SR/OSR) declines, thus overemphasizing contrastive learning loss may lead the agent to prioritize modality alignment over core sequential navigation tasks.

7.5. Overall Design on R2R

We further supplemented the performance of each key component of SUSA on the R2R task. As shown in Tab. 6, our previous conclusions are reaffirmed: the DSP module allows the agent to better perceive spatial layouts, thus improving navigation efficiency (SPL). The TSU module is better at understanding textual semantics, resulting in higher success rates. After integrating the DSP and TSU modules, the agent’s performance improved significantly (e.g., SR=73.05, SPL=64.85). When the HRA module is further introduced, the navigation success rate on R2R increases to 73.95, indicating that contrastive learning further enhances instruction-environment alignment. However, its SPL metric remains suboptimal, suggesting that the contrastive learning strategy in the HRA module may excel at accurately aligning the environment with instructions but lacks the capability to optimize the navigation path length.

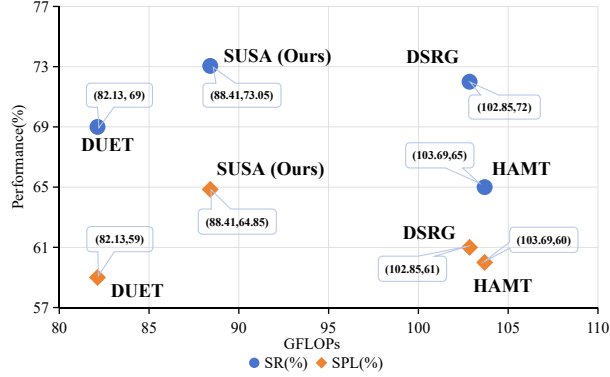


Figure 10. Comparison of computational efficiency and navigation performance on R2R validation unseen split with several popular VLN methods.

7.6. Computing Efficiency vs. Navigation Performance

As Fig. 10 illustrated, we compare the Giga Floating-point Operations (GFLOPs) and navigation performance (*i.e.*, SR/SPL, which are more important metrics) of different VLN models, including DUET [6], DSRG [50], HAMT [5] and our SUSA. To ensure a fair comparison across all methods, we performed single-step forward inference with a batch size of 8, an instruction length of 44, and 6 exploration map nodes. Compared to the baseline DUET, our approach introduces spatial and semantic environmental information, which inevitably increasing computational cost. However, benefiting from the partial pretraining strategy and a shared panorama encoder for both the depth and RGB environmental information, our SUSA architecture notably enhances agent navigation performance with modest computational resources. The frozen BLIP-2 and CLIP models provide the agent with off-the-shelf textual semantics and are excluded from the training or inference.

8. Qualitative Examples

Failure cases. We provide an in-depth examination of failure cases, aiming to offer valuable insights for future model improvements. Fig. 11 displays the difference between the navigation trajectory predicted by the proposed SUSA and the ground truth trajectory. We found that, although textual semantics can provide the agent with a richer understanding, it may introduces ambiguity in certain scenarios. Concretely, when two identical salient landmarks appear in different scenes (*e.g.*, the staircase and bathroom in Fig. 11), the agent may struggle to distinguish the correct navigable node, leading to erroneous navigation decisions.

More Qualitative Examples. We further visualize first-person navigation trajectories on the R2R validation unseen split, as illustrated in Fig. 12.

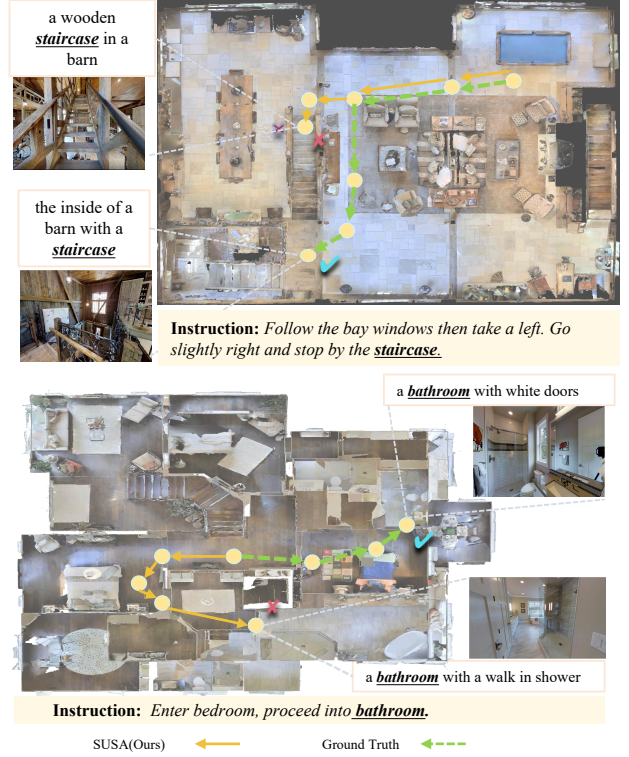


Figure 11. Top-down trajectories visualization of failed cases. The corresponding instructions are shown at the bottom. Partial views of final stopping position and corresponding landmark captions of ground truth and SUSA are also provided

9. Limitations and Future Work

As previously mentioned, when an agent encounters the same landmark at different navigable points, it may struggle to make confident navigation decisions, leading to failures. To address this limitation, 1) our future research will explore adjusting the confidence levels associated with different environmental representations to help the agent make more accurate and reliable predictions. 2) Beyond landmarks, we will construct direction-related textual semantics (*e.g.*, "past," "turn left") to better model the spatial relationships between actions in instructions and the environmental layout or historical exploration maps.

In the future, we also intend to explore the generalizability of our approach, which integrates richer representations from multiple perspectives, in embodied tasks such as continuous navigation and embodied question answering. Additionally, given the complexity of VLN tasks, current mainstream VLN frameworks are often intricate and cumbersome, with a wide variety of evaluation metrics that are difficult to balance. Ongoing research in the future is expected to develop more lightweight VLN model architectures and comprehensive evaluation metrics.



Instruction: Turn around and go to the left. Turn right and cross through the kitchen. At the end of the hallway stop.



Instruction: Go straight and make a sharp left then go towards the living room where you will see a photo frame of the nyc skyline

Figure 12. First-person trajectory visualizations of DUET (left) and our SUSAN (right), with the corresponding instructions provided below. Red arrows indicate the next selected viewpoint from current position.